Applied Catalysis B: Environmental 190 (2016) 75–84

Contents lists available at ScienceDirect

Applied Catalysis B: Environmental

journal homepage: www.elsevier.com/locate/apcatb

Confinement of Ag_3PO_4 nanoparticles supported by surface plasmon resonance of Ag in glass: Efficient nanoscale photocatalyst for solar H_2 production from waste H_2S

Santosh S. Patil[a,b], Deepak R. Patil[a], Sanjay K. Apte[a], Milind V. Kulkarni[a], Jalindar D. Ambekar[a], Chan-Jin Park[c,*], Suresh W. Gosavi[d], Sanjay S. Kolekar[b], Bharat B. Kale[a,*]

[a] Centre for Materials for Electronics Technology (C-MET), Department of Electronics and Information Technology (DeitY), Government of India, New Delhi, Panchawati Off Pashan Road, Pune 411008, India
[b] Analytical Chemistry and Material Science Research Laboratory, Department of Chemistry, Shivaji University, Kolhapur, India
[c] Department of Materials Science and Engineering, Chonnam National University 77, Yongbongro, Bukgu, Gwangju, Republic of Korea
[d] Department of Physics, Savitribai Phule Pune University, Ganeshkhind, Pune 411007, India

ARTICLE INFO

Article history:
Received 3 December 2015
Received in revised form 24 February 2016
Accepted 29 February 2016
Available online 2 March 2016

Keywords:
Ag_3PO_4 Glass nanocomposite
H_2S Splitting
Photocatalytic
Recycle

ABSTRACT

Ag_3PO_4 is a good photocatalyst but ubiquitously known for its photocorrosion problem during photocatalytic reaction. Therefore, stabilization of Ag_3PO_4 with retaining its fundamental properties has immense importance. With this motivation, we designed Ag_3PO_4 glass nanocomposite to resolve the problem of photocorrosion. Moreover, the effect of size quantization on photocatalytic activity has also been demonstrated by growing the cubic Ag_3PO_4 nanoparticles with size in the range of 3–9 nm in glass matrix via melt and quenching method. The band gap of Ag_3PO_4 has been tuned (2.56–2.25 eV) in glass matrix with respect to size. Considering the size tunable band gap of Ag_3PO_4 glass nanocomposite within visible region, it is demonstrated as a photocatalyst for hydrogen (H_2) production from copious hazardous waste H_2S. The utmost H_2 production i.e. 3920.4 $\mu mol\, h^{-1}\, g^{-1}$ is obtained using 1 gm of Ag_3PO_4 glass nanocomposite powder. The apparent quantum yield for H_2 production is calculated to be 5.51% for Ag_3PO_4 glass nanocomposite. Interestingly, presence of plasmonic Ag was also observed in Ag_3PO_4 glass nanocomposite which contributes for H_2 production through enhanced light absorption, efficient charge separation and improved stability. Recycling study of sample reveals stable H_2 production efficiency and good stability of the photocatalyst. Surprisingly, catalyst can be reused many times and recovery of catalyst is possible just rinsing with distilled water. All these results demonstrate directly the feasibility of designing a new generation photocatalysts.

1. Introduction

In recent years, semiconductor quantum dots (QDs) are considered as an important class of materials in numerous fundamental and applied areas of nanotechnology [1] due to their unique physical and chemical properties [2], particularly for their ability to store excess electrons and holes [3], changes in electronic properties upon surface modifications [4] and large absorption coefficients [5,6] etc. Nevertheless, from physicochemical viewpoint, effective control over size, shape and morphology of QDs during synthesis is very crucial in order to achieve the desired properties for material [7]. To circumvent these problems, one effective strategy is to employ a suitable flexible matrix such as silica (SiO_2) glass to accommodate II–VI semiconductor for production of optically useful nanoparticles in a robust and stable form [8,9]. Generally, silicate and borosilicate glasses were exploited as a host material to study diffusion controlled growth of semiconductor in glass matrix. Importantly, it is proclaimed that the glass matrix surrounding semiconductor nanoparticles play an important role in structural phase transition and for conferring unusual optical properties [9–11].

So far, cadmium chalcogenide (CdX(X = S,Se,Te)) based glass nanocomposites have been reported extensively because of their wide applications with band gap energies covering a wide range

* Corresponding authors.
E-mail addresses: parkcj@jnu.ac.kr (C.-J. Park), bbkale1@gmail.com (B.B. Kale).

http://dx.doi.org/10.1016/j.apcatb.2016.02.068
0926-3373/

of wavelengths from ultraviolet to near infrared region exhibiting high photoluminescence quantum yield [10–12]. Similarly, Cd chalcogenide silica glass nanocomposites are commercially available in the form of yellow-to-red sharp-cut off filters [9,12]. Amongst them, CdS-doped glasses are well known because of its extended use as phosphor, photovoltaic cell, field effect transistor, hetero-junction laser, acoustic amplifier, etc. [5,13,14]. There is plenty of room in the area of semiconductor glass nanocomposites to attempt the approaches like metal doping in order to modify the properties of pristine semiconductor. For example, recently, Dantas et al. [15] have demonstrated Mn doped CdS i.e. $Cd_{1-x}Mn_xS$ nanoparticles in glasses which showed superior size tunable optical and magnetic properties. Thus, previous study indicates that the presence of glass surrounding is advantageous and could be helpful to enhance the physicochemical properties of material remarkably.

Nevertheless, upto now, the use of Cd chalcogenide glass nanocomposites were limited, only for its optical and photonic applications [16,17]. An important breakthrough has established for Cd chalcogenide glass nanocomposites since it was used as a photocatalyst for photocatalytic H_2 production from H_2S splitting [18–20]. Interestingly, Cd chalcogenide glass nanocomposites were indeed found to be very stable and efficient photocatalysts for H_2 production compared to their bulk material counterpart [20]. However, the use of cadmium (Cd) has become a major concern for commercial applications due to its toxicity. Moreover, the use of materials consisting of heavy metals such as Cd, Hg, and Pb has been banned in many regions of the world [21,22] and therefore, scientists throughout world are looking for Cd free materials.

In this light, we have tried to prepare Cd free glass nanocomposites by using semiconductor oxide silver phosphate (Ag_3PO_4) which has similar optical properties to those of CdS. Ag_3PO_4 semiconductor has an indirect band gap of 2.36 eV and a direct band gap of 2.43 eV, which make it potential candidate for visible light driven photocatalytic applications in organic pollutant degradation as well as for water splitting [23,24]. However, there are still some inherent shortcomings in Ag_3PO_4 like it is light-sensitive and slightly soluble in aqueous solution, which makes it photocorrosive [25,26]. That means, under prolonged light irradiation Ag_3PO_4 is prone to photoreduction and decomposes if no sacrificial reagent is supplied [26]. In the past, various Ag_3PO_4 coupled semiconductor composite systems were exemplified like $Ag_3PO_4/TiO_2/Fe_3O_4$ [25], Graphene oxide/Ag_3PO_4 [26], $Ag_3PO_4/NiFe_2O_4$ [27], Co_3O_4/Ag_3PO_4 [28] etc., in order to improve the photocatalytic activity by improving the stability and separation of photogenerated charge carriers. Although, such composite systems showed enhanced photocatalytic activity, the stability problem of Ag_3PO_4 has not been resolved completely. All the above studies report the synthesis of catalysts by wet chemical method and the photocatalytic stability of the photocatalysts was examined with their recyclable ability for consecutive photocatalytic experiments. To the best of our knowledge, there were no any synthesis route of using matrices was designed for stabilizing Ag_3PO_4. Moreover glass matrix helps to control the dimensions of Ag_3PO_4 particles, which can tune the physical as well as optical properties of the photocatalyst. Previously, it has been indeed shown that confinement effect of semiconductor in glass matrix provides new insight for controlling charge transfer in photocatalysis [29,30]. So, an attempt has been made to design the Ag_3PO_4 glass nanocomposite to resolve the problem of photocorrosion as well as investigate the size dependent photocatalytic activities.

Photocatalytic H_2 production from H_2S splitting has proved to be excellent approach to solve global energy and environment problems [18–20,31]. H_2S is considered as an environmental pollutant because of its toxic and malodorous nature. Every year abundant H_2S is produced (15–20%) around the world from the natural gas deposits and petroleum refineries [20]. Hence, the decomposition of H_2S has importance for the production of H_2 and to curtail the environmental pollution problem.

The present work describes the rational design of Ag_3PO_4 glass nanocomposite which was further extensively characterized in order to examine their structural and optical properties. The plausible photocatalytic H_2S splitting reaction mechanism has also been derived. The recyclability (stability) of the Ag_3PO_4 glass nanocomposite photocatalyst is also evaluated by recovering and reusing catalyst after photocatalytic reaction.

2. Experimental

2.1. Synthesis of Ag_3PO_4 based glass nanocomposite

In the present work, we have designed a new glass composition for synthesis of Ag_3PO_4 glass nanocomposite. Firstly, Ag_3PO_4 powder was synthesized by hydrothermal method. In typical procedure, solution of Ag_3PO_4 (0.3 M) (AR grade, SDFCL) was added drop wise to the solution $NH_4H_2PO_4$ (0.1 M) (Qualigens Chemicals) under vigorous stirring at room temperature. Then the entire solution was transferred in Teflon vessel, which was fitted into a stainless steel hydrothermal reactor and kept at 100 °C for 8 h. After reaction the reactor was allowed to cool naturally and the product obtained was washed thoroughly with water, filtered, dried and used for further characterization. The as synthesized Ag_3PO_4 powder was used further for preparation of Ag_3PO_4 glass nanocomposite.

Two types of Ag_3PO_4 doped silica glass nanocomposites were prepared by making slight variations in the glass compositions: (i) AP glasses- Ag_3PO_4 doped silica glasses without addition of ammonium dihydrogen phosphate ($NH_4H_2PO_4$) and (ii) APD glasses- Ag_3PO_4 doped silica glasses with addition of $NH_4H_2PO_4$ in place of TiO_2 in the previous glass composition. The starting glass forming composition for the synthesis of Ag_3PO_4 embedded glass was 60 SiO_2, 6 Na_2O, 15.5 K_2O, 8 ZnO, 2 TiO_2, 3 B_2O_3 and 5.5 BaO (all in wt.%, Qualigens Chemicals). All the raw materials and 0.4 wt.% Ag_3PO_4 were mixed thoroughly in ball milling to obtain homogeneous mixture. It was melted in an electrically heated furnace at 1250 °C for 3 h and air quenched on previously heated brass plate. The as casted glass blank was treated as an unstriked glass. The doped glass nanocomposites have been striked (heat treated) at different temperatures in order to study the effect of temperature on crystallization of Ag_3PO_4 in the glass matrix. The AP glass nanocomposites were striked at temperatures 525, 550, 575 °C for 8 h and were labelled as AP525, AP550, AP575, respectively. The APD glass nanocomposites striked at temperatures 510, 520, 530, 540 °C for 8 h were named as APD510, APD520, APD530 and APD540, respectively. Bright yellow colored Ag_3PO_4 glass nanocomposite was obtained (Fig. 1 and Fig. 2). Several controlled experiments were performed in order to optimize Ag_3PO_4 glass nanocomposite with homogeneous yellow colouration and good transparency (Supporting Information Table S1 and Fig. S1). As synthesized Ag_3PO_4 glass nanocomposite samples were subjected to various physicochemical characterizations. The Ag_3PO_4 glass nanocomposite was then ground to a fine powder for TEM and photocatalysis studies.

2.2. Characterization

X-ray diffraction techniques were used to carry out the structural characterization of as prepared Ag_3PO_4. The X-ray diffraction (XRD) studies of the sample was performed by (XRD-D8, Advanced Bruker-AXS) using Cu Ka (1.5406 nm) radiation. The sample was scanned in 2θ range from 10 to 80°. Raman spectrum of the Ag_3PO_4 glass nanocomposite was performed using HR 800-Raman Spectroscopy, Horiba JobinYvon, France. UV–vis-near infrared spectrometer (UV-VIS-NIR, Perkin Elmer Lambda-950) was used

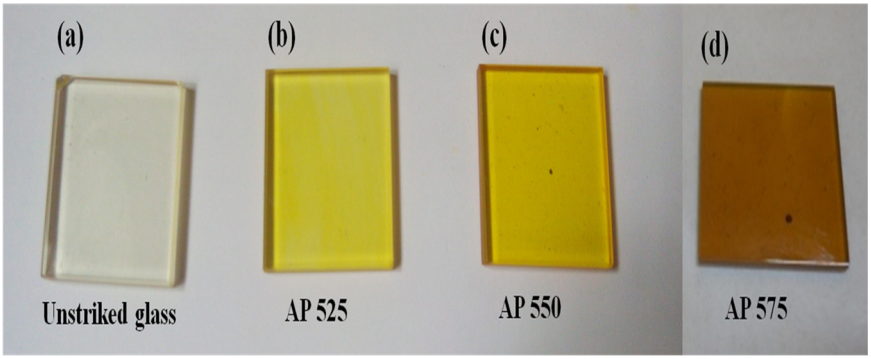

Fig. 1. Photograph of (a) Unstriked glass nanocomposite (b) AP 525 (c) AP550 (d) AP575 samples.

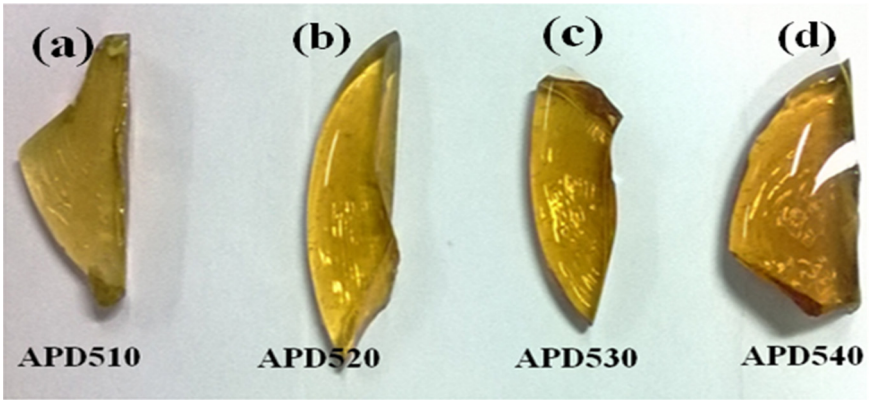

Fig. 2. Photograph of (a) APD510 (b) APD520 (c) APD530 (d) APD540 samples.

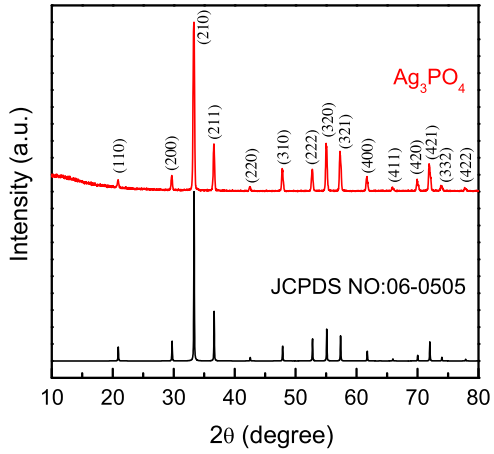

Fig. 3. XRD pattern of Ag_3PO_4 powder.

to study the optical properties of Ag_3PO_4 glass nanocomposites. Photoluminescence study was performed by using Flurolog-3 Spectroflurometer, HORIBA SCIENTIFIC. FESEM (Hitachi S-4800 II) was used to study the morphology. High resolution morphological studies were performed with (HRTEM, JEOL, 2010F).

2.3. Photocatalytic H_2S splitting

1 g of the photocatalyst (Ag_3PO_4 glass nanocomposite powder of grain size of −120/+250 μ) was introduced as a suspension into a cylindrical quartz reactor. A Xe-lamp light source (LOT ORIEL GRUPPEEUROPA, LSH302) of intensity 300 W with cut-off filter (>420 nm) was used to cut off the light in the ultraviolet region. At a constant temperature 25 (±1 °C), the vigorously stirred suspension was purged with argon for 1 h and then hydrogen sulphide (H_2S) was bubbled through the solution for about 1 h. Each experiment was carried out using 1 g of photocatalyst in 750 ml of KOH solution (0.5 M) with H_2S flow 2.5 ml min^{-1}. The excess hydrogen sulphide was trapped in NaOH solution. The amount of produced H_2 was measured using graduated gas burette and gas chromatograph (Model Shimadzu GC-14B, MS-5 Å column, TCD, Ar carrier). The apparent quantum yield efficiency for H_2 generation is calculated by using equation (1) given below,

$$\text{A.Q.E}\,(\%) = \frac{(\text{Number of } H_2 \text{ molecules evolved} \times 2)}{(\text{Number of incident photon})} \times 100 \qquad (1)$$

The details for the calculation of quantum yield efficiency are given in Supporting Information S2.

3. Results and discussion

As synthesized Ag_3PO_4 powder has been used as a semiconductor dopant for preparation of Ag_3PO_4 glass composite. The concentration of Ag_3PO_4 powder was optimized to around 0.4 wt.% in the glass composition. Experimental observations showed that higher concentration of Ag_3PO_4 leads to inhomogeneous and heavy precipitation throughout the glass (Supporting Information, Table S1). Any glass composition does not accommodate more than 0.5 wt.% doping because of the imbalance in the glass composition which leads into glass ceramics (opaque) with heavy precipitation. However, homogeneous and transparent Ag_3PO_4 glass nanocomposites sample were obtained with 0.4 wt.% of Ag_3PO_4. Therefore, 0.4 wt.% of Ag_3PO_4 doped glass nanocomposites have been used for further studies. Stepwise representation of different processes used during synthesis of Ag_3PO_4 glass nanocomposite is also given for

better understanding the procedure. (See Supporting Information, Fig. S1).

3.1. XRD analysis of Ag_3PO_4

X-ray diffraction (XRD) pattern (Fig. 3) showed formation of single phase highly crystalline Ag_3PO_4 with cubic crystal structure (a = 6.004 Å). The XRD pattern is well matched with the standard JCPDS data (JCPDS No.06-0505). The presence of high intensity peaks clearly reveals the good crystallinity of Ag_3PO_4. Morphological features of pure Ag_3PO_4 powder were investigated by FESEM that showed formation of micron sized rhombic dodecahedrons. (Supporting Information Fig. S3). XRD pattern of Ag_3PO_4 nanoparticle embedded glass nanosystem did not show any remarkable peaks due to very low concentration of Ag_3PO_4 in glass matrix. The broad peak (in the 2θ range of 25–35) was appeared in XRD that attributed due to silica glass. (Supporting Information, Fig. S4). In view of this, the existence of the Ag_3PO_4 nanoparticles in glass nanocomposite is further supported and confirmed by RAMAN, HRTEM and UV–vis spectroscopy study.

3.2. Transmission electron microscopy (TEM) analysis

TEM analysis was used to measure the particle sizes, size distribution and crystal structure of Ag_3PO_4. TEM micrograph of the AP525 and AP550 glass nanocomposites were shown in Fig. 4a and b, respectively. From the TEM micrographs, it is clear that Ag_3PO_4 nanoparticles are homogeneously distributed in the glass matrix. The appearance of bright yellow color throughout the glass is also an indication of uniform growth of Ag_3PO_4 nanoparticles in the glass matrix (Fig. 1 and Fig. 2). TEM analysis reveals the formation of around 3–4 nm sized Ag_3PO_4 nanoparticles in AP525 and 5–6 nm in AP550 glass nanocomposite samples, respectively. Hence, minimum 3 nm sized Ag_3PO_4 nanoparticles with monodispersion can be grown in the glass matrix. AP575 glass nanocomposite showed comparatively larger particle size in the range of 8–13 nm which can also be evidenced from slight dark reddish color of composite. This further purported that the crystal growth is dependent on striking temperature given to quenched glass nanocomposites.

High resolution TEM (HRTEM) image of AP575 (Fig. 4d) showed clear lattice fringes with an interplanar spacing of 0.24 nm that corresponds to (211) crystallographic plane Ag_3PO_4 thus consistent with the XRD pattern, which is also evident from the corresponding selected-area electron diffraction (SAED) pattern (inset to Fig. 4c). The faint hallow rings with occasional bright spot in SAED pattern suggests the growth of cubic Ag_3PO_4 in silica glass matrix.

SAED pattern and HRTEM images of APD series Ag_3PO_4 glass nanocomposite samples are also shown in Fig. 5(a–h). After careful observation of HRTEM images, very tiny nanoparticles of Ag_3PO_4 can be seen in the glass with uniform distribution. The growth of Ag_3PO_4 nanoparticles of size distribution around 4, 5, 7 and 9 nm (Fig. 5a–h) has been observed for the sample APD510, APD520, APD530 and APD540, respectively. Hence, minimum 4 nm sized Ag_3PO_4 nanoparticles with monodispersion can be grown in the glass matrix. Two apparent rings in SAED pattern (Fig. 5g) correspond to cubic Ag_3PO_4 (210), and (420) planes, respectively, which are in good agreement with the XRD pattern of Ag_3PO_4 nanopowder. The calculated inter-planer spacing from lattice fringes of HRTEM images shows consistency with XRD results of Ag_3PO_4 nanopowder.

In the present study our objective was to grow very tiny nanoparticles in glass matrix without disturbing the optical quality of the glass. Hence, the striking temperatures have been selected to obtain smaller nanoparticles with homogeneous distribution. The temperature above 575 °C conferred heavy precipitation of Ag_3PO_4 with bigger particle size in glass matrix and diminishes the transparency.

3.3. Raman study

Raman spectroscopy is an important tool and generally used to identify the presence of semiconductor in glass matrix [32]. The crystallization of Ag_3PO_4 nanoparticles in the glass matrix was investigated by using Raman spectroscopy. Fig. 6a and b depicts raman spectra of Ag_3PO_4 glass nanocomposites (AP and APD series). The Raman spectrum of pristine Ag_3PO_4 powder is shown in Fig. 6a which exhibits only one sharp peak at around 908 cm^{-1} [33,34]. On the other hand, two distinct peaks were observed for AP and APD series Ag_3PO_4 glass nanocomposite samples. The first peak at 900 cm^{-1} corresponds to the Ag_3PO_4 nanoparticles while the second peak at 1100 cm^{-1} is a characteristic peak of alkali silicate glass [35]. Raman spectrum of host glass was also recorded which showed only one peak around 1100 °C that attributed to alkali silicate glass (Supporting Information, Fig. S5) [35] Raman study clearly reveals that nanoparticles formed inside the silica glass matrix are comprised of Ag_3PO_4.

3.4. Optical study

Optical absorption is an excellent probe for the electronic bandgap determination; originated as a result of electron excitation from semiconductor by the incident photon. The selective optical absorption of Ag_3PO_4 nanoparticles in glass due to confinement effect helps to investigate the nucleation and growth of Ag_3PO_4 nanoparticles. The dimensions of Ag_3PO_4 was continuously shrinks down to the nanometer or smaller scale which led to change in physical, optical and electronic properties termed as quantum size effects. Therefore, confinement of Ag_3PO_4 can drastically alter the fundamental properties of Ag_3PO_4. Fig. 7a, depicts the UV–vis transmittance spectra of unstriked glass, AP525, AP550 and AP575 samples. A sharp optical spectrum was observed at 330 nm for unstriked glass which corresponds to band gap of 3.66 eV. The glass nanocomposite sample AP525 showed absorption edge around 486 nm which correspond to band gap value 2.56 eV and consistent with the band gap of pristine Ag_3PO_4. It can be clearly seen that the optical cut-off edge shifted towards red with the increase of striking temperature leading to shift in the band gap from 2.56 eV to 2.25 eV. This can be attributed to the increase in size of the Ag_3PO_4 nanoparticles with increasing striking temperature. Surprisingly, a considerable anomalous hump was observed at wavelength of 350 nm for glass nanocomposite samples AP525 and AP550 and it was further disappeared for glass striked at higher temperature i.e., 575 °C. The anomalous hump observed in the spectra can be attributed to the growth of atomic Ag which results in deficiency of PO_4^{2-} during the growth of Ag_3PO_4. Although, the hump disappears completely at striking temperature of 575 °C, glass becomes translucent (color changes to blackish red) due to formation of bigger sized Ag_3PO_4 nanoparticles in the glass matrix.

In order to obtain the uniform growth of Ag_3PO_4 in glass matrix and to maintain high transparency the composition of host glass was modified (APD glass) by addition of $NH_4H_2PO_4$. Different amounts of $NH_4H_2PO_4$ (0.5–4 wt.%) were added and optimized (2%) in the specially designed glass composition. Experimental observations suggest that the concentration of $NH_4H_2PO_4$ (>2%) makes glass nanocomposite opaque (blackish) due to uncontrolled rapid growth of Ag_3PO_4 since $NH_4H_2PO_4$ itself acts as a good nucleating agent in glass. However, $NH_4H_2PO_4$ concentration less than 2% is not sufficient to obtain complete growth of Ag_3PO_4 in silica glass matrix. Finally, homogeneous yellow coloured transparent Ag_3PO_4 glass nanocomposite samples were obtained with 2 wt.%

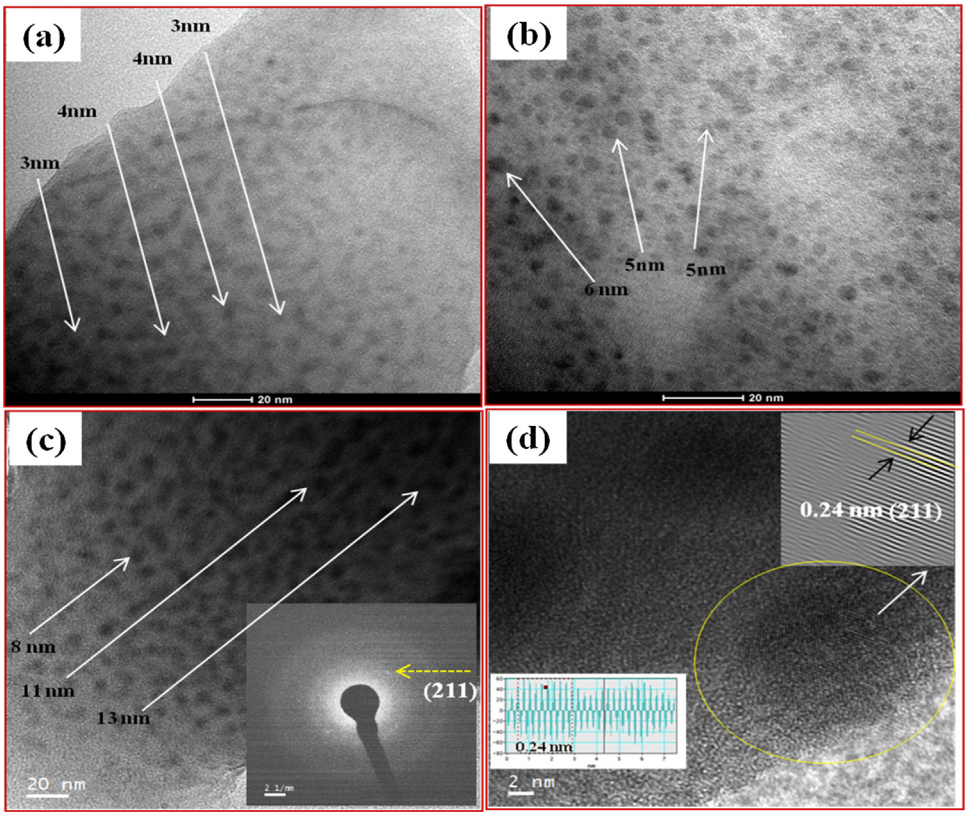

Fig. 4. TEM images of (a) AP 525, (b) AP 550 and (c, d) HRTEM images of AP 575. Inset of Fig. 4c shows the SAED pattern of AP 575.

Table 1
Glass sample description and parameters.

Sample ID	Description	Optical cut off (nm)	Band gap (eV)
Unstriked glass	Unstriked glass	330	3.66
AP525	Striked at 525 °C for 8 h	484	2.56
AP550	Striked at 550 °C for 8 h	500	2.48
AP550R*	Striked at 550 °C for 8 h	500	2.48
AP 575	Striked at 575 °C for 8 h	552	2.25
APD510	Striked at 510 °C for 8 h	489	2.53
APD510R*	Striked at 510 °C for 8 h	489	2.53
APD520	Striked at 520 °C for 8 h	500	2.48
APD530	Striked at 530 °C for 8 h	516	2.39
APD540	Striked at 540 °C for 8 h	531	2.33

of $NH_4H_2PO_4$. In this way, the amount of $NH_4H_2PO_4$ was optimized in glass composition. An added of $NH_4H_2PO_4$ in present case provides extra PO_4^{2-} ions to the dissolved ionic Ag^+ in the glass matrix. With the addition of $NH_4H_2PO_4$, we found that the intensity of the anomalous hump centered at 350 nm was drastically reduced (Fig. 7b). The absorption edges for Ag_3PO_4 glass nanocomposites APD510, APD520, APD530 and APD540 were observed to be 489 nm, 500 nm, 516 nm and 531 nm, respectively, corresponding to the band gap energies of 2.54, 2.49, 2.41, and 2.33 eV, respectively (Table 1).

The band gap value of 2.33 eV was observed for sample APD 540, which is lower than bulk, Ag_3PO_4 powder (2.45 eV) as obtained from UV–vis transmission spectra. (Supporting Information, Fig. S6). The observed shift in the band gap as compared to bulk powder is due to presence of glass matrix [18]. The overall band gap of nanoparticles is entirely dependent on the band gap energy of the matrix. Baskoutas and Terzis [36] have shown experimentally and theoretically, the effect of glass matrix on the overall band gap of CdS QDs. The internal lattice strain developed by the doping is also responsible for shift in the bandgap. Such incorporation of the dopant induces the internal lattice strain due to the size and charge difference. The red shift caused by the lattice strain competes with the blue shift due to quantum size effect and the overall effect is the slight decrease in the bandgap [18]. Hence, all quantum dots embedded glass systems shows slight shift in band gap.

To study the radiative recombination and separation efficiency of photogenerated electrons and holes (e^-/h^+), photoluminescence (PL) spectra of AP and APD glass nanocomposite samples were acquired. Fig. 8a and b shows the room temperature PL spectra of AP and APD series glass nanocomposite samples recorded using excitation wavelength of 350 nm. The strong emission band is observed at around 420 nm, which is arise from the recombination of the charge-transfer transition between the O2p orbital and the empty d orbital of the central Ag^+ or of the self-trap excitons in the PO_4 oxyanion complex [37,38]. The broad PL band observed from 500 to 600 nm is originated from the radiative recombination of photo-generated holes with electrons around the surface oxygen vacancies [38]. The emission band centered at around 550 nm has photon energy approximately equal to that of band gap of Ag_3PO_4 [38]. The intensities of photoluminescence spectra were found to be increased with thermal treatment; probably due to the increased growth of Ag_3PO_4 nanoparticles in the glass [10]. In addition, it should be noted that the higher temperature and long heat treatment increases the total concentration of Ag_3PO_4 nanoparticles, which in turn exhibit higher intensity.

It is widely accepted that lower the intensity of PL spectrum lower is the recombination of e^-/h^+ pairs. Among all the samples, APD510 showed lowest intensity of emission peak, indicating the low recombination of e^-/h^+ on the surface of photocatalyst and longest life time therefore exhibiting better photocatalytic efficiency. This indicates that the charge carriers recombination in

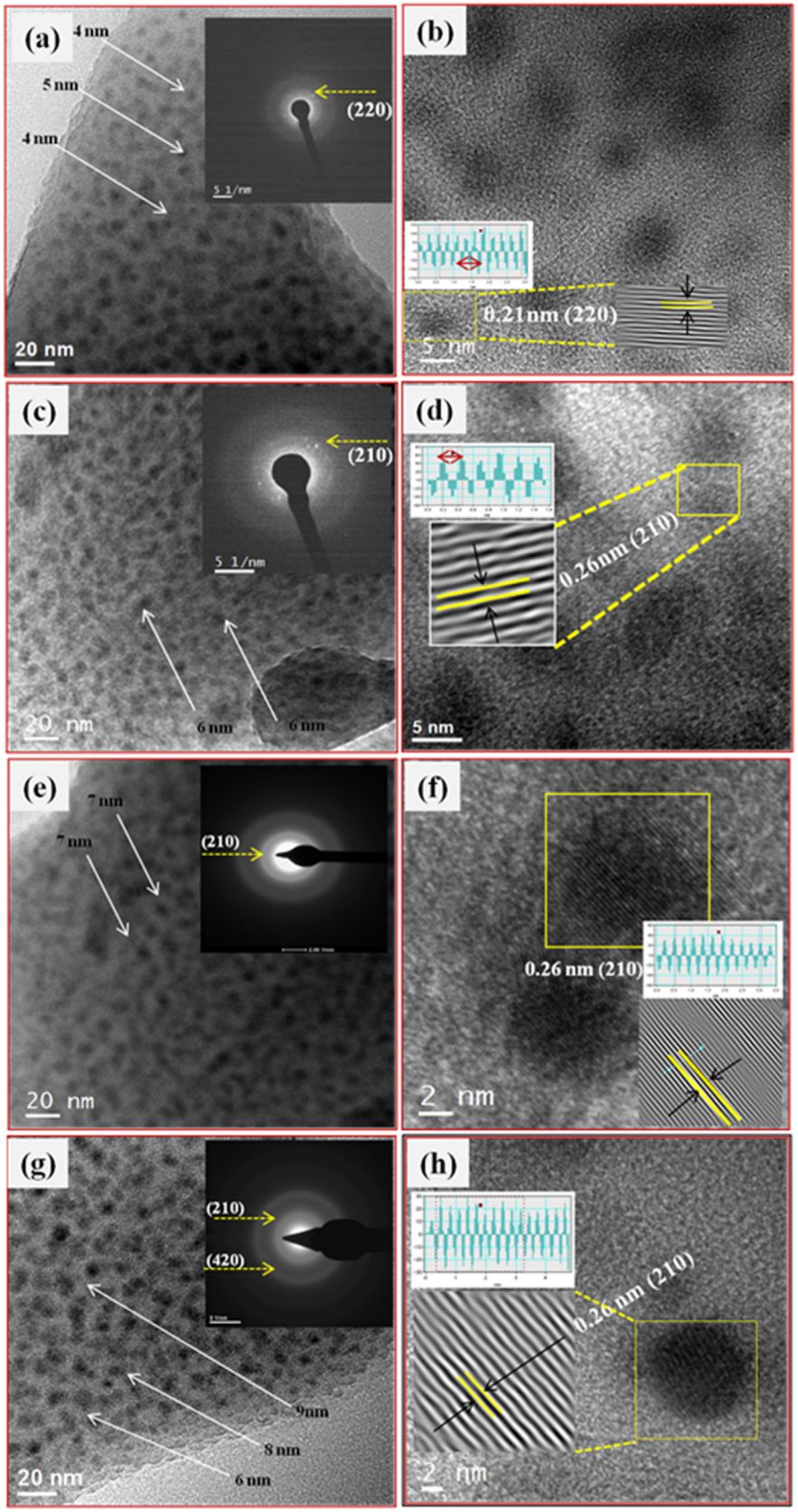

Fig. 5. HRTEM images of (a, b) APD 510, (c, d) APD 520, (e, f) APD 530 and (g, h) APD 540 samples. Insets show the SAED patterns of respective samples.

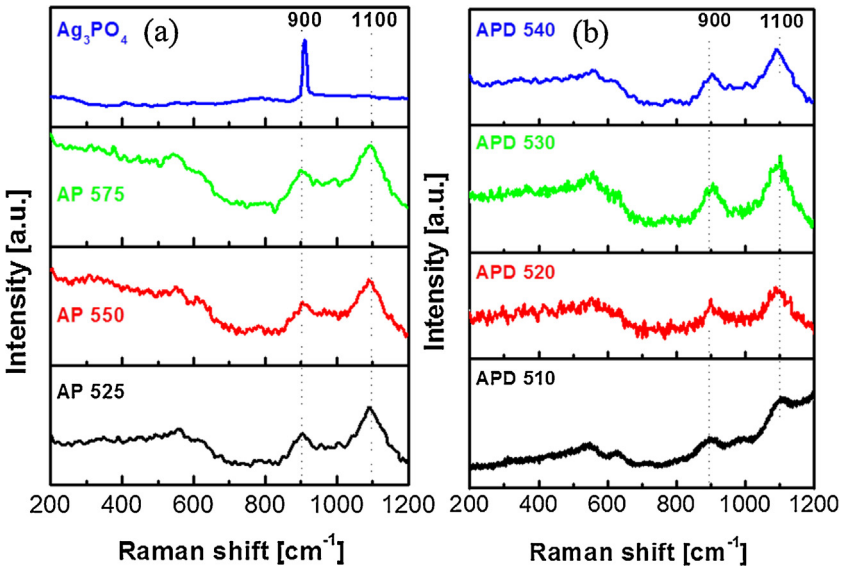

Fig. 6. Raman spectra of (a) Ag_3PO_4, AP525, AP550, AP575 (b) APD510, APD520, APD530, APD540 glass nanocomposite samples.

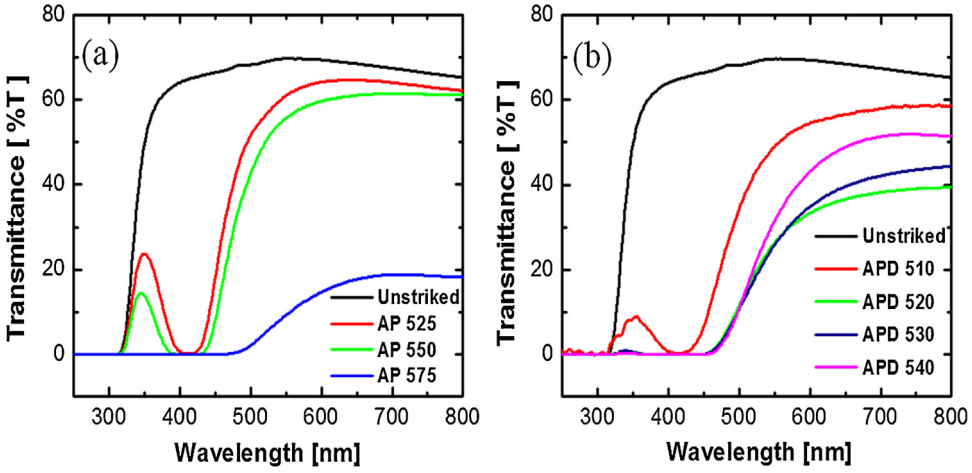

Fig. 7. UV–vis spectra of (a) Unstriked glass, AP525, AP550, AP575 (b) Unstriked glass, APD510, APD520, APD530 APD540 glass nanocomposite samples, respectively.

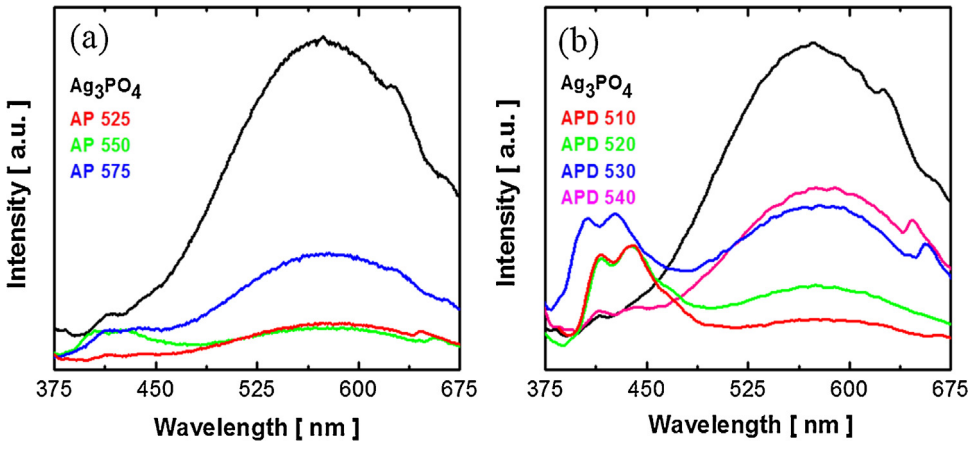

Fig. 8. PL spectra of (a) Ag_3PO_4, AP525, AP550, AP575 (b) Ag_3PO_4, APD510, APD520, APD530, APD540 glass nanocomposite samples, respectively.

Ag_3PO_4 glass nanocomposite was increased with heat treatment i.e., increase in nanoparticle size and suppress the recombination at lower particle size [39].

3.5. Growth mechanism

The formation of Ag_3PO_4 nanoparticles in silica glass matrix by melt and quench technique invites discussion for the reaction and

growth mechanism. Crystal growth of semiconductor in a silica glass matrix is a thermodynamic process of precipitation from a supersaturated solution; occurs in different stages such as i) nucleation of semiconductor clusters, ii) normal growth coalescence of nuclei and iii) cluster induced devitrification of bulk glass process [40]. In present study, Ag_3PO_4 has been used as a dopant for preparation Ag_3PO_4 glass nanocomposite. Firstly, the semiconductor dopant Ag_3PO_4 is present in ionic form in the glass matrix. Ag^+ and PO_4^{3-} ions are randomly distributed in the quenched glass sample. When as synthesized glass is heat treated near to its glass transition temperature crystal growth of Ag_3PO_4 occurs. During heat treatment process, Ag^+ and PO_4^{3-} ions come closer to form Ag_3PO_4 nuclei as per the following reaction.

$$3Ag^+ + PO_4^{3-} \text{-------} Ag_3PO_4(\text{nuclei}) \quad (2)$$

The schematic representation of Ag_3PO_4 nanoparticles growth mechanism in glass matrix is shown in Scheme S1 (Supporting Information). At initial striking temperature tiny Ag_3PO_4 nuclei were generated in the supersaturated solid solution of glass. Growth of these Ag_3PO_4 nuclei is accelerated by prolonged heat treatment at higher temperature and further crystal growth occurs as per the standard crystal growth mechanism i.e., Ostwald ripening as a function of striking temperature and time [9,40]. After prolonged thermal treatment these tiny particles are self organized in the glass matrix to form stable Ag_3PO_4 nanoparticles. The observed crystal growth is extremely slow due to the silica glass matrix atmosphere. These newly formed tiny particles were spontaneously aggregated to minimize their surface energy. The Ag_3PO_4 particle size increases with increasing striking temperature and time leading to formation of particles with average size from a few to several nanometers [8]. The confinement of Ag_3PO_4 nanoparticles with respect to striking temperature in glass matrix could be another reason for increase in particle size [20]. The growth mechanism in aqueous solution and glass is quite different. In glass it is taking place just above the transition and below the softening temperature of glass. During heat treatment, the mobility of the ions increased with temperature and time within the glass regime. The movement of ions is very slow and hence required more time (in hrs) for formation of nuclei and further nanoparticles.

3.6. Photocatalytic H_2 production

As stated earlier, Ag_3PO_4 is a well-known visible light active photocatalyst, however restricts its practical use due to photocorrosion problem. Hence, we have tried to check its stability by constructing their composite with glass matrix and evaluated their photocatalytic activities. The band gap of Ag_3PO_4 glass nanocomposite was found to be narrow, in the range of 2.56–2.33 eV, which falls well within the visible region and makes these glass nanocomposites promising candidates as a visible light active photocatalyst. Here, we examined visible light induced photocatalytic H_2S splitting for H_2 production using Ag_3PO_4 glass nanocomposite photocatalysts. The glass nanocomposite samples were crushed into fine powders prior to study their photocatalytic H_2S splitting. It is important to note that the H_2 production from the crushed Ag_3PO_4 glass nanocomposite is mainly attributed to exposed Ag_3PO_4 nanoparticles at the edge surface of the glass particles [19]. Due to presence of surrounding glass matrices, Ag_3PO_4 particles are adhering to the surface and well protected. It is further note that no porosity or voids take part in H_2 production. SEM images are provided for more clarity (See Supporting Information, Fig. S7). Fig. 9a and b depicts time dependent H_2 production from H_2S splitting using AP and APD samples, respectively. The linearity of the graphs clearly shows the consistent evolution of H_2 from H_2S splitting using Ag_3PO_4 glass nanocomposite photocatalyst. The photocatalyst sample (1 gm of naked Ag_3PO_4 glass nanocomposite powder) contains 0.04 gm of Ag_3PO_4 which confer excellent H_2 production. The utmost H_2 production i.e., 3677 μmol h^{-1} g^{-1} and 3920 μmol h^{-1} g^{-1} were obtained for AP525 and APD510 photocatalyst samples, respectively (Table 2). This indicates lower nanoparticle sized glass samples showed higher H_2 production rate and as the particle size increases H_2 production rate decreases. Hence, the better H_2 production rate is obtained for AP525 (3–4 nm) and APD510 (3–5 nm) photocatalyst samples, is quite justifiable.

The reason is AP525 and APD510 photocatalyst samples have comparatively smaller particle size of Ag_3PO_4 in the range of 3–4 nm and (3–5 nm) offering more exposed area for the light absorption. Therefore, more number of Ag_3PO_4 nanoparticles

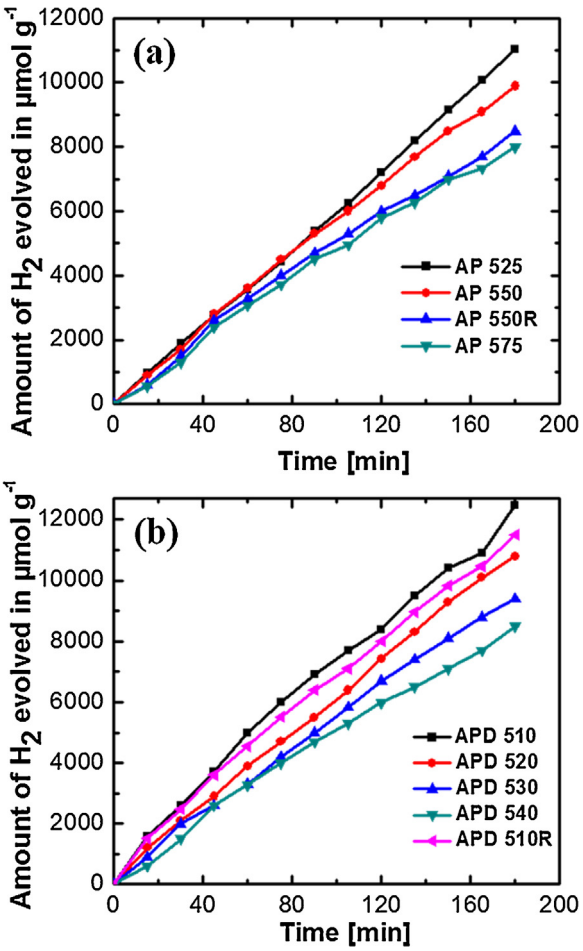

Fig. 9. Photocatalytic activities of (a) AP525, AP550, AP550R, AP575 (b) APD510, APD510R, APD520, APD530, APD540 glass samples, respectively.

Table 2
Photocatalytic activities for H_2 evolution from H_2S.

Sample ID	Particle size (nm)	Amt. of H_2 evolved in μmol h^{-1} g^{-1}	Apparent quantum yield efficiency (AQE (%))
Ag_3PO_4 powder	Submicron	Nil (Photocorrosion problem)	Nil
Unstriked glass	Nil	Nil	Nil
AP525	3–4	3677	5.17
AP550	5–6	3297	4.64
AP550R	5–6	2831	3.97
AP 575	8–13	2665	3.74
APD510	3–5	3920.4	5.51
APD510R	3–5	3809.4	5.35
APD520	4–6	3678.6	5.16
APD530	6–7	3250.4	4.55
APD540	6–9	2914.8	4.09

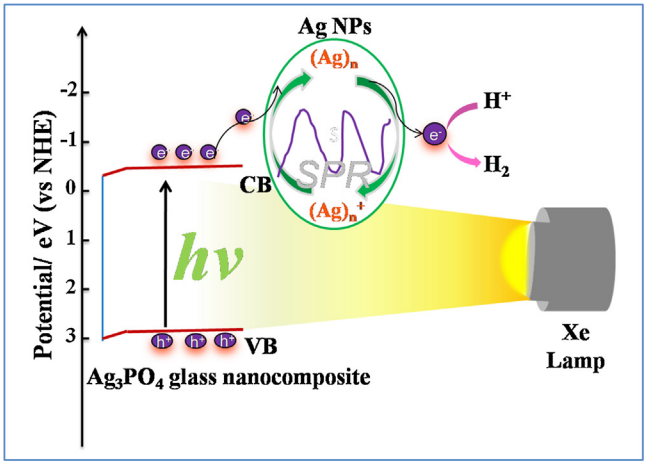

Fig. 10. Reaction mechanism for photocatalytic H_2 evolution over Ag_3PO_4 glass nanocomposite.

would get exposed to light irradiation owing to the formation of more charge carriers. As evidenced from the optical study, presence of plasmonic Ag in Ag_3PO_4 glass nanocomposite accelerates the photocatalytic performance since Ag can trap electron and retard the charge recombination [41–43]. The photoluminescence study shows the great inhibition of charge carrier recombination in case of Ag_3PO_4 glass nanocomposite with lower particle size which justifies its higher photocatalytic activity. It is important to note that H_2 would not be formed over pristine Ag_3PO_4, since the potential of the conduction band of Ag_3PO_4 (+0.285 eV V_{NHE}) is insufficient for proton reduction. On the other hand, in case of Ag_3PO_4 glass nanocomposite, the proton was getting reduced at Ag sites producing H_2 due to ability of Ag to reduce H^+. The expected working mechanism for photocatalytic H_2 formation over Ag_3PO_4 glass nanocomposite is shown in Fig. 10 which involves different steps. (i) Initially, Ag nanoparticles absorb the incident photon through their SPR excitation [44] (ii) Meanwhile; the Ag_3PO_4 also absorbs incident photon and produces electrons in conduction band (CB) and holes in valence band (VB). (iii) The photoexcited electrons are transferred from CB of Ag_3PO_4 to the electron deficient Ag nanoparticles, returning to original state. Then the electrons at the surface of Ag reduce H^+, resulting into formation of H_2. Since, hydrogen overvoltage of Ag metal (−0.22 V) is more negative than that of pristine Ag_3PO_4 (+0.285 eV V_{NHE}), the H_2 evolution over Ag is quite favorable and reasonable [44–46]. Overall, the presense of Ag in Ag_3PO_4 glass nanocomposite keeping the electron potential negative (transfer of electron from Ag_3PO_4 to Ag) is very important and key for H_2 formation over Ag_3PO_4 under visible light irradiation. Sadale et al. [47] and Nasere et al. [48] have independently worked for Pt/WO_3 and Ag/WO_3 photocatalysts wherein similar problem of positive band edge potential (+0.5 V_{NHE}) for H_2 formation was appeared. These research groups have reported that the presence plasmonic metal like Pt, Ag act as an electron collecter providing negative redox potential that consequently reduces H^+ to form H_2. It is apparent that combination of plasmonic effect of Ag with narrow band gap of Ag_3PO_4 accelerate the light absorption by utilizing both SPR and band gap excitation as well as provides the negative potential for electron to produce H_2.

Moreover, from thermodynamic point of view, photocatalytic H_2S splitting to produce H_2 requires much less energy whereas photocatalytic H_2O splitting requires huge amount of energy. The energy required for these two processes is different.

Gibbs free energy of formation [49] i.e.,

For H_2O: $\Delta G^\circ = 237.19$ kJ/mol

($E^\circ = -\Delta G^\circ/2F = -1.23$ eV)

For H_2S: $\Delta G^\circ = 33.44$ kJ/mol

($E^\circ = -\Delta G^\circ/2F = -0.17$ eV)

In H_2S decomposition the E° is −0.17 which is quite less negative compared to H_2O splitting [44]. The photocatalytic H_2S splitting reactions using Ag_3PO_4 glass nanocomposite are given below,

$$Ag_3PO_4 glass nanocomposite \xrightarrow{hv,\lambda>420nm} h^+_{VB} + e^-_{CB} \quad (2)$$

$$H_2S + OH^- \xrightarrow{alkali} HS^- H_2O \quad (3)$$

$$2HS^- + 2\,h^+_{VB} \rightarrow 2H^+ + S_2^{2-} (\text{oxidation reaction}) \quad (4)$$

$$2H^+ + 2e^-_{CB} \rightarrow H_2 \uparrow (\text{Reduction reaction}) \quad (5)$$

The photocatalytic H_2S splitting reaction takes place as follows. In 0.5 M KOH solution with pH of 12.5–13.0, the weak diprotic acid H_2S dissociates and maintains equilibrium with hydrosulphide HS^- ions. The Ag_3PO_4 glass nanocomposite absorbs light energy equivalent to its band gap energy and generates (e^-/h^+) pairs. As stated earlier, the photoinduced electrons get transferred to plasmonic Ag which provide reaction site to reduce H^+ and produce H_2. The photogenerated valence band holes (h^+_{VB}) oxidizes the HS^- ions into disulfide ions (S_2^{2-}), liberating a proton from the HS^- ions. We did not observe H_2 production in dark as well as in absence of photocatalyst indicates that H_2 production is due to Ag_3PO_4. Interestingly, we have carried out H_2S splitting without KOH but we found that H_2 production is quite negligible. The blank run i.e., without H_2S at similar experimental conditions did not produce H_2 indicating that H_2 production in present case is mainly from H_2S and not from H_2O.

H_2S splitting using pristine Ag_3PO_4 powder was also carried out and showed degradation of Ag_3PO_4 during photocatalytic reaction giving negligible H_2 production. When Ag_3PO_4 bulk powder was directly exposed to light, it becomes black due to photocorrosion. In contrast, Ag_3PO_4 glass nanocomposite retains its stability (yellow color) even after exposing to light irradiation for longer time (See Supporting Information, Fig. S8). This indicates that the surrounding glass layer (matrix) plays a significant role in order to give stability for Ag_3PO_4. This might be due to the fact that the glass matrix holds the Ag_3PO_4 crystals by internal glass former network which further protects Ag_3PO_4 and suppress the photocorrosion. Thus, Ag_3PO_4 glass nanocomposite sample conferred stable photocatalytic activity for H_2 production from H_2S. The photocatalytic stability of Ag_3PO_4 glass nanocomposite was reconfirmed by reusing it over replicate photocatalytic reaction for H_2 production (Fig. 9b, result of APD510R). The Ag_3PO_4 glass nanocomposite showed consistent photocatalytic H_2 evolution for recyclable experiments with good stability. As evidenced from the acquired Raman spectrum of recycled photocatalyst sample, (APD510R) the consistency observed in the spectrum clearly indicates photocatalyst sample is recoverable, robust and reusable (Supporting Information, Fig. S9). The above results indicate that glass matrix plays a key role in order to stabilize the Ag_3PO_4 nanoparticles, since it has ability to accommodate and relax strain which is observed at the surface of nanoparticles [50]. Moreover, the reduced dimensions of Ag_3PO_4 down to the nanometer scale or smaller scale might also lead to stability of Ag_3PO_4 in glass nanocomposite.

4. Conclusion

In a nutshell, we have investigated Ag_3PO_4 glass nanocomposite for H_2 production from copious waste H_2S for the first time. The band gap of Ag_3PO_4 was tuned from 2.25 eV to 2.56 eV in the glass matrix by precisely controlling the striking temperature. The effect of size quantization on photocatalytic activity was examined. The utmost H_2 production i.e., 3920.4 μmol $h^{-1}g^{-1}$ is obtained for APD510 sample having particle size of 3–5 nm. The combination

effect of surface plasmonic Ag along with Ag_3PO_4 is responsible for H_2 production through enhanced light absorption, efficient charge separation and improved stability. More significantly, this photocatalyst can be recycled easily and reused for replicate photocatalysis experiments. Considering all these, it becomes obvious that H_2, the fuel of future when produced from H_2S, brings forth the twin benefits of a sustainable energy resource and aesthetic environmental pollution abatement.

Acknowledgements

Authors would like to thank Department of Electronics and Information Technology (DeitY, New Delhi), for financial support. Bharat Kale and Chan-Jin Park are also thankful for the support by MSIP (Ministry of Science, ICT and future planning), Korea through Brain Pool Program. Authors are thankful to Nanocrystalline material and Glass laboratory, C-MET Pune. Author also acknowledges an additional support from UGC-SAP Department of Chemistry, Shivaji University Kolhapur for their generous help.

Appendix A. Supplementary data

Supplementary data associated with this article can be found, in the online version, at http://dx.doi.org/10.1016/j.apcatb.2016.02.068.

References

[1] R. Beaulac, P.I. Archer, S.T. Ochsenbein, D.R. Gamelin, Adv. Funct. Mater. 18 (2008) 3873.
[2] A. Henglein, J. Phys. Chem. 97 (1993) 5457.
[3] A. Henglein, A. Fojtik, H. Weller, Ber. Bunsenges. Phys. Chem. 91 (1987) 441.
[4] L. Spanhel, M. Haase, H. Weller, J. Am. Chem. Soc. 109 (1987) 5649.
[5] B. Julian, J. Planelles, E. Cordoncillo, P. Escribano, P. Aschehoug, C. Sanchez, B. Vianab, F. Pelle, J. Mater. Chem. 16 (2006) 4612.
[6] C. Giansante, I. Infante, E. Fabiano, R. Grisorio, G.P. Suranna, G. Gigli, J. Am. Chem. Soc. 137 (2015) 1875.
[7] L.-Y. Chen, J.-Q. Xu, H. Choi, H. Konishi, S. Jin, X.-C. Li, Nat. Commun. 5 (2014) 3879.
[8] T.M. Hayes, L.B. Lurio, J. Pant, P.D. Persans, Solid State Commun. 117 (2001) 627.
[9] Y.M. Azhniuk, A.V. Gomonnai, Y.I. Hutych, V.V. Lopushansky, I.I. Turok, V.O. Yukhymchuk, D.R.T. Zahn, J. Cryst. Growth 312 (2010) 1709.
[10] G.R. Olbright, N. Peyghambarian, Appl. Phys. Lett. 48 (1986) 1184.
[11] C. Liu, J. Heo, X. Zhang, J.L. Adam, J. Non Cryst. Solids 354 (2008) 618.
[12] V.I. Klimov, A.A. Milhailovsky, S. Xu, A. Malko, J.A. Hollingsworth, C.A. Leatherdale, H.-J. Eisler, M.G. Bawendi, Science 290 (2000) 314.
[13] A. Chahboun, A.G. Rolo, S.A. Filonovich, M.J.M. Gomes, Sol. Energy Mater. Sol. Cells 90 (2006) 1413.
[14] E.O. Serqueira, N.O. Dantas, G.H. Silva, V. Anjos, M.J.V. Bell, M.A. Pereira-da-Silva, Chem. Phys. Lett. 504 (2011) 67.
[15] N.O. Dantas, E.S.F. Neto, R.S. Silva, D.R. Jesus, F. Pelegrini, Appl. Phys. Lett. 93 (2008) 193115.
[16] N.F. Borelli, D.W. Hall, H.J. Holl, D.W. Smith, J. Appl. Phys. 61 (1987) 5399.
[17] H. Yukselici, P. Pearsans, T. Hayes, Phys. Rev. B: Condens. Matter 52 (1995) 11763.
[18] S.K. Apte, S.N. Garaje, M. Valant, B.B. Kale, Green Chem. 14 (2012) 1455.
[19] B.B. Kale, J.-O. Baeg, S.K. Apte, R.S. Sonawane, S.D. Naik, K.R. Patil, J. Mater. Chem. 17 (2007) 4297.
[20] S.K. Apte, S.N. Garaje, S.D. Naik, R.P. Waichal, J.-O. Baeg, B.B. Kale, Nanoscale 6 (2014) 908.
[21] N.L. Pickett, S. Daniels, Patent PCT/GB2006/004003 (2006).
[22] N.L. Pickett, S. Daniels, I. Mushtaq, Patent UK/GB2007/0714865.3. 2007.
[23] B. Yingpu, S. Ouyang, N. Umezawa, J. Cao, J. Ye, J. Am. Chem. Soc. 133 (2011) 6490.
[24] Z. Yi, J. Ye, N. Kikugawa, T. Kako, S. Ouyang, H. Stuart-Williams, H. Yang, J. Cao, W. Luo, Z. Li, Y. Liu, R.L. Withers, Nat. Mater. 9 (2010) 559.
[25] J.-W. Xu, Z.-D. Gao, K. Han, Y. Liu, Y.-Y. Song, Appl. Mater. Interfaces 6 (2014) 15122.
[26] L. Liu, J. Liu, D. Delai Sun, Catal. Sci. Technol. 2 (2012) 2525.
[27] S.S. Patil, M.S. Tamboli, V.G. Deonikar, G.G. Umarji, J.D. Ambekar, M.V. Kulkarni, B. Kale, S.S. Kolekar, D.R. Patil, Dalton Trans. 44 (2015) 20426.
[28] C. Tang, E. Liu, J. Wan, X. Hu, J. Fan, Appl. Catal. B: Environ. 181 (2016) 707.
[29] F.A. Frame, F.E. Osterloh, J. Phys. Chem. C 114 (2010) 10628.
[30] D. Tanaka, Y. Oaki, H. Imai, Chem. Commun. 46 (2010) 5286.
[31] S. Baykara, H. Figen, A. Kale, T. Veziroglu, Int. J. Hydrogen Energy 32 (2007) 1246.
[32] P.D. Persans, L.B. Lurio, J. Pant, H. Yukselici, G.D. Lian, T.M. Hayes, J. Appl. Phys. 87 (2000) 3850.
[33] T.L.R. Hewer, B.C. Machado, R.S. Freire, R. Guardani, RSC Adv. 4 (2014) 34674.
[34] P. Dong, Y. Wang, B. Cao, S. Xin, L. Guo, J. Zhang, F. Li, Appl. Catal. B: Environ. 132 (2013) 45.
[35] D.W. Matson, S.K. Sharma, J.A. Philpotts, J. Non Cryst. Solids 58 (1983) 323.
[36] S. Baskoutas, A. Terzis, J. Appl. Phys. 99 (2006) 013708.
[37] J.J. Liu, X.L. Fu, S.F. Chen, Y.F. Zhu, Appl. Phys. Lett. 99 (2011) 1919031.
[38] X. Ma, B. Lu, D. Li, R. Shi, C. Pan, Y. Zhu, J. Phys. Chem. C 115 (2011) 4680.
[39] Q. Liang, Y. Shi, W. Ma, Z. Li, X. Yang, Phys. Chem. Chem. Phys. 14 (2012) 15657.
[40] J. Yang, M. Gao, Y. Zhang, L. Yang, J. Lang, D. Wang, H. Liu, Y. Liu, Y. Wang, Superlattices Microstruct. 44 (2008) 137.
[41] L.-C. Liu, S.H. Risbud, J. Appl. Phys. 68 (1990) 28.
[42] S.S. Patil, R.H. Patil, S.B. Kale, M.S. Tamboli, J.D. Ambekar, W.N. Gade, S.S. Kolekar, B.B. Kale, J. Nanopart. Res. 16 (2014) 11.
[43] Y. Zheng, C. Chen, Y. Zhan, X. Lin, Q. Zheng, K. Wei, J. Zhu, J. Phys. Chem. C 112 (2008) 107.
[44] A. Tanaka, K. Hashimoto, H. Kominami, J. Am. Chem. Soc. 136 (2014) 586.
[45] Y.A. Attia, D. Buceta, C. Blanco-Varela, M.B. Mohamed, G. Barone, M.A. Loípez-Quintela, J. Am. Chem. Soc. 136 (2014) 1182.
[46] H. Kominami, A. Furusho, S.-Y. Murakami, H. Inoue, Y. Kera, B. Ohtani, Catal. Lett. 76 (2001) 31.
[47] S.B. Sadale, K. Noda, K. Kobayashi, K. Matsushige, Phys. Status Solidi C 8 (2011) 552.
[48] N. Naseri, H. Kim, W. Choi, A.Z. Moshfegh, Int. J. Hydrogen Energy 38 (2013) 2117.
[49] J.-O. Baeg, A novel nanoscale semiconductor photocatalyst for solar hydrogen production, Proc. SPIE (2008), http://dx.doi.org/10.1117/2.1200810.1328.
[50] T.M. Hayes, L.B. Lurio, P.D. Persans, Phys. Rev. B 63 (2001) 155417.